ACADEMIC PRESS

Available online at www.sciencedirect.com

SCIENCE DIRECT®

Journal of Solid State Chemistry 173 (2003) 122–129

JOURNAL OF SOLID STATE CHEMISTRY

http://elsevier.com/locate/jssc

Crystal growth, structural characterization and magnetic properties of Ca_3CuRhO_6, $Ca_3Co_{1.34}Rh_{0.66}O_6$ and Ca_3FeRhO_6

Matthew J. Davis, Mark D. Smith, and Hans-Conrad zur Loye*

Department of Chemistry and Biochemistry, University of South Carolina, 631 Sumter Street, Columbia, SC, 29208, USA

Received 30 October 2002; received in revised form 17 January 2003; accepted 18 January 2003

Abstract

Single crystals of Ca_3CuRhO_6, $Ca_3Co_{1.34}Rh_{0.66}O_6$ and Ca_3FeRhO_6 were synthesized by high temperature flux growth in molten K_2CO_3 and structurally characterized by single crystal X-ray diffraction. While $Ca_3Co_{1.34}Rh_{0.66}O_6$ and Ca_3FeRhO_6 crystallize with trigonal (rhombohedral) symmetry in the space group $R\bar{3}c$, $Z = 6$: $Ca_3Co_{1.34}Rh_{0.66}O_6$ $a = 9.161(1)$ Å, $c = 10.601(2)$ Å; Ca_3FeRhO_6 $a = 9.1884(3)$ Å, $c = 10.7750(4)$ Å; Ca_3CuRhO_6 adopts a monoclinic distortion of the K_4CdCl_6 structure in the space group $C2/c$, $Z = 4$: $a = 9.004(2)$ Å, $b = 9.218(2)$ Å, $c = 6.453(1)$ Å, $\beta = 91.672(5)$. All crystals of Ca_3CuRhO_6 examined were twinned by pseudo-merohedry. Ca_3CuRhO_6, $Ca_3Co_{1.34}Rh_{0.66}O_6$, and Ca_3FeRhO_6 are structurally related and contain infinite one-dimensional chains of alternating face-sharing RhO_6 octahedra and MO_6 trigonal prisms. In the monoclinic modification, the copper atoms are displaced from the center of the trigonal prism toward one of the rectangular faces adopting a pseudo-square planar configuration. The magnetic properties of Ca_3CuRhO_6, $Ca_3Co_{1.34}Rh_{0.66}O_6$, and Ca_3FeRhO_6 are discussed.

© 2003 Elsevier Science (USA). All rights reserved.

Keywords: Crystal growth; Oxides; Crystal structure; Magnetic properties; Ca_3CuRhO_6; $Ca_3Co_{1.34}Rh_{0.66}O_6$; Ca_3FeRhO_6

1. Introduction

In the recent literature, there have been numerous contributions discussing the structures and characterizations of transition metal oxides with 2H-perovskite related structures, generally described by the formula $A_{3n+3m}A'_nB_{3m+n}O_{9m+6n}$. The interest in this class of oxide materials is due to the fact that many of these compounds exhibit intriguing structural and magnetic properties, which has prompted recent work by many groups to prepare numerous compositions containing different metal cations in a range of oxidation states [1]. The structures are all derived from the stacking of mixed $[A_3O_9]$ and $[A_3A'O_6]$ layers in the c-direction, as described by Darriet and Subramanian [2]. Subsequent filling of the interstitial octahedral sites with B cations leads to a structural family with the general formula $A_{3n+3m}A'_nB_{3m+n}O_{9m+6n}$, where n/m is the ratio between the number of $[A_3O_9]$ and $[A_3A'O_6]$ layers [2,3]. The $m = 0$, $n = 1$ member of this family, $A_3A'BO_6$, crystallizes in the K_4CdCl_6 structure type, the prototype of which, Sr_4PtO_6, was first prepared by Randall and Katz [4]. This structure type consists of infinite one-dimensional chains of alternating face-sharing trigonal prisms and octahedra along the c-axis. These chains, in turn, are separated by chains of the alkaline-earth cations, which are found in a distorted square antiprismatic coordination.

Most of the $m = 0$, $n = 1$ compositions crystallize with rhombohedral symmetry, as observed for the parent compound. The introduction of copper into the A' site, however, causes a change in the structure [5–16], ensuing from the coordination preference of copper. The copper is displaced from the pseudo-threefold axis towards one of the rectangular faces of the trigonal prism, adopting a distorted square planar geometry. The polyhedral chains in this monoclinic phase, consequently, consist of alternating octahedra and square planes. A comparison of the chains containing $[MO_6]$ trigonal prisms and those that contain $[CuO_4]$ square planes is shown in Fig. 1.

Although many compounds belonging to this family have been synthesized, the majority of them have been prepared as polycrystalline powders. A major breakthrough in the synthesis of oxides of this family came through the application of molten salts [1] or fluxes to grow single crystals [17] and several research groups

---

*Corresponding author. Fax: +1-803-777-8508.
E-mail address: zurloye@sc.edu (H.-C. zur Loye).

0022-4596/03/$ - see front matter © 2003 Elsevier Science (USA). All rights reserved.
doi:10.1016/S0022-4596(03)00102-6

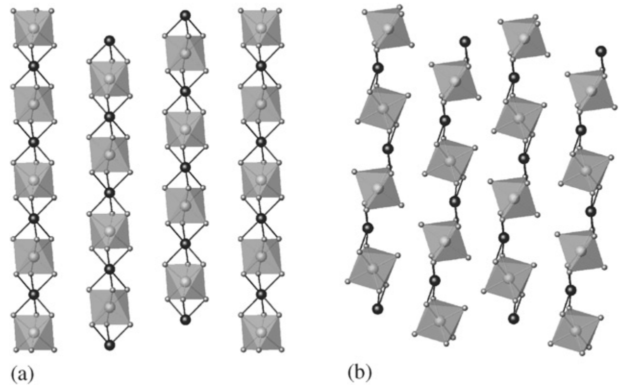

Fig. 1. A comparison of the structures of Ca_3FeRhO_6 (a) and Ca_3CuRhO_6 (b). In Ca_3FeRhO_6 (a) the polyhedral chains consist of alternating RhO_6 octahedra and FeO_6 trigonal prisms. Ca_3CuRhO_6 (b) consists of alternating RhO_6 octahedra and CuO_4 square planes. In both figures, RhO_6 octahedra are represented by shaded grey polyhedra and Cu or Fe are represented as black spheres. Calcium atoms are omitted for clarity.

have been very successful in growing single crystals from molten alkali carbonates [6,18,19], hydroxides [20–23], and chlorides [22,24–26]. Research within our group has focused on the systematic preparation of single crystals via high temperature flux growth using hydroxide and carbonate melts [1,5,6,27–32].

Recently, there has been much interest in $Ca_3Co_2O_6$ [18,33–38], an $m = 0$, $n = 1$ member of this family where Co occupies both the A' and B sites. The magnetic properties of both polycrystalline and single crystal samples are complex and studies on single crystals established that $Ca_3Co_2O_6$ consists of a triangular lattice of ferromagnetic chains that couple antiferromagnetically. These investigations have sparked interest in compositionally related compounds, resulting in the synthesis and characterization of $Ca_3Co_{1+x}Ir_{1-x}O_6$ [35], $Ca_3Co_{1+x}Ru_{1-x}O_6$ [35], Ca_3FeRhO_6 [39], and Ca_3CoRhO_6 [39].

In this paper, we report the synthesis and magnetic characterization of Ca_3CuRhO_6 and $Ca_3Co_{1.34}Rh_{0.66}O_6$, two new $m = 0$, $n = 1$ members of this group, as well as the crystal growth condition and single crystal structural determination of Ca_3FeRhO_6. Although the latter has been previously synthesized as a polycrystalline powder [39], up to now, no reports detailing the growth of single crystals of this oxide has been reported in the literature. The magnetic properties of Ca_3CuRhO_6 and $Ca_3Co_{1.34}Rh_{0.66}O_6$ are also reported.

2. Experimental

2.1. Crystal growth

Single crystals of Ca_3CuRhO_6, $Ca_3Co_{1.34}Rh_{0.66}O_6$, and Ca_3FeRhO_6 were grown from a molten K_2CO_3 flux. $CaCO_3$ (Alfa Aesar, 99.95%), CuO (Cerac, 99.999%) or Co_3O_4 (Alfa Aesar, 99.7%) or Fe_2O_3 (Johnson Matthey, 99.999%), and Rh metal (Engelhard, 99.9995%) in a molar ratio of 3:1:1 were mixed thoroughly and placed in an alumina crucible followed by an addition of a ten-fold mass excess of K_2CO_3 flux. The filled crucibles were then covered and heated in air at a rate of $10°C\,min^{-1}$ to 1050°C, held at that temperature for 24 h, and cooled at a rate of $0.25°C\,min^{-1}$ to 850°C, at which point the furnace was shut off. Crystals of Ca_3MRhO_6 ($M =$ Cu, Co, Fe) were separated from the flux by washing with water, aided by the use of sonication. Several crystals suitable for single crystal X-ray diffraction were isolated manually under a microscope.

2.2. Structure determination

Single crystals of the title compounds were epoxied onto the end of thin glass fibers. X-ray intensity data were measured at 293 K on a Bruker SMART APEX CCD-based diffractometer (Mo$K\alpha$, $\lambda = 0.71073$ Å) [40]. The raw data frames were integrated with the Bruker SAINT+ program [40], which also applied corrections for Lorentz and polarization effects. Analysis of the data showed negligible crystal decay during data collection. Empirical absorption corrections based on the multiple measurement of equivalent reflections were applied with the program SADABS [40].

Systematic absences in the intensity data for $Ca_3Co_{1.34}Rh_{0.66}O_6$ and Ca_3FeRhO_6 were consistent with the space group $R\bar{3}c$. Positional and thermal parameters corresponding to the K_4CdCl_6 structure type were refined by full-matrix least-squares against F^2, using the SHELXTL software package [41]. All atoms were refined with anisotropic displacement parameters. The structural refinement of Ca_3CuRhO_6 was carried out in the space group $C2/c$ based on previously determined isotypic compounds. All of the several Ca_3CuRhO_6 crystals examined exhibited broader diffraction maxima than ideal. All showed three-fold twinning ("trilling") by pseudo-merohedry with a pseudo-rhombohedral cell. The twinning in Ca_3CuRhO_6 is exactly analogous to that previously observed in Sr_3CuPtO_6 [16], in which a thorough discussion of the possible twin elements for this structural modification is presented. The refinement of the Ca_3CuRhO_6 data employed the absent rhombohedral three-fold axis as the twin element. The twin law in matrix notation used is (by rows): (0.5 −0.5 1/0.5 −0.5 −1/0.5 0.5 0). The final refined twin fractions for the three domains are 0.28/0.25/0.47. Despite the twin treatment, the relatively high R factors may be because of the lower crystal quality or because of the presence of additional twinning, as described by Hodeau et al. [16]. Relevant

Table 1
Crystal data and structure refinement for Ca_3CuRhO_6, $Ca_3Co_{1.34}Rh_{0.66}O_6$, and Ca_3FeRhO_6

Empirical formula	Ca_3CuRhO_6	$Ca_3Co_{1.34}Rh_{0.66}O_6$	Ca_3FeRhO_6
Formula weight ($g\,mol^{-1}$)	382.69	363.13	375.00
Space group	$C2/c$	$R\bar{3}c$	$R\bar{3}c$
Unit cell dimensions			
a (Å)	9.004(2)	9. 161(1)	9.1884(3)
b (Å)	9.218(2)	9. 161(1)	9.1884(3)
c (Å)	6.453(1)	10.601(2)	10.7750(4)
α (deg)	90	90	90
β (deg)	91.672(5)	90	90
γ (deg)	90	120	120
Volume (Å^3)	535.35(16)	770.5(2)	787.82(5)
Z	4	6	6
Density (calculated) ($Mg\,m^{-3}$)	4.748	4.696	4.742
Absorption coefficient (mm^{-1})	9.889	9.401	8.793
$F(000)$	728	1043	1074
Crystal size (mm^3)	$0.10 \times 0.07 \times 0.05$	$0.12 \times 0.07 \times 0.04$	$0.16 \times 0.10 \times 0.07$
$2\theta_{max}$ (deg)	30.50	37.75	37.75
Index ranges	$-12 \leqslant h \leqslant 12, -12 \leqslant k \leqslant 13, -9 \leqslant l \leqslant 7$	$-14 \leqslant h \leqslant 13, -15 \leqslant k \leqslant 10, -18 \leqslant l \leqslant 14$	$-6 \leqslant h \leqslant 15, -15 \leqslant k \leqslant 14, -14 \leqslant l \leqslant 18$
Reflections collected	3113	2274	2901
Independent reflections	863 ($R_{int} = 0.1843$)	462 ($R_{int} = 0.0289$)	473 ($R_{int} = 0.0287$)
Goodness-of-fit on F^2	1.103	1.142	1.122
Final R indices ($I > 2\sigma(I)$)	$R_1 = 0.0709$, w$R_2 = 0.1799$	$R_1 = 0.0223$, w$R_2 = 0.0532$	$R_1 = 0.0217$, w$R_2 = 0.0497$
R indices (all data)	$R_1 = 0.0730$, w$R_2 = 0.1814$	$R_1 = 0.0261$, w$R_2 = 0.0544$	$R_1 = 0.0234$, w$R_2 = 0.0506$
Residual electron density (e^- Å^{-3})	2.369/ −2.677	1.032/ −1.445	1.261/−1.712

Table 2
Atomic coordinates and equivalent isotropic displacement parameters for Ca_3CuRhO_6, $Ca_3Co_{1.34}Rh_{0.66}O_6$, and Ca_3FeRhO_6, respectively. U(eq) is defined as one third of the trace of the orthogonalized U^{ij} tensor

	x	y	z	U(eq) (Å^2)	Occupancy
Ca_3CuRhO_6					
Ca(1)	0	0.8960(3)	1/4	0.0123(7)	1
Ca(2)	0.3129(2)	0.9250(2)	0.6218(3)	0.0102(5)	1
Cu	0	0.3049(2)	1/4	0.0143(5)	1
Rh	1/4	1/4	1/2	0.0080(4)	1
O(1)	0.1407(10)	0.0715(10)	0.4325(16)	0.0144(18)	1
O(2)	0.2183(10)	0.3162(9)	0.2067(15)	0.0146(17)	1
O(3)	0.4447(8)	0.1522(8)	0.4542(13)	0.0115(15)	1
$Ca_3Co_{1.34}Rh_{0.66}O_6$					
Ca	0.36758(5)	0	1/4	0.0088(1)	1
Co(1)	0	0	1/4	0.0101(1)	1
Co(2)	0	0	0	0.0064(1)	0.34(3)
Rh	0	0	0	0.0064(1)	0.66(3)
O	0.1798(2)	0.0244(2)	0.1147(1)	0.0110(2)	1
Ca_3FeRhO_6					
Ca	0.36854(5)	0	1/4	0.0072(1)	1
Fe	0	0	1/4	0.0063(1)	1
Rh	0	0	0	0.00467(9)	1
O	0.1791(2)	0.0216(2)	0.1195(1)	0.0099(2)	1

crystallographic data for the three materials are compiled in Table 1, atomic positions are listed in Table 2, and selected interatomic distances are summarized in Tables 3 and 4.

2.3. Magnetism

The magnetic susceptibilities of loose crystals of Ca_3CuRhO_6, $Ca_3Co_{1.34}Rh_{0.66}O_6$, and Ca_3FeRhO_6 were measured using a Quantum Design MPMS XL SQUID magnetometer. The samples were measured under both zero field cooled (ZFC) and field cooled (FC) conditions in applied fields of 0.5, 5, and 40 kG over the temperature range of $2\,\text{K} \leqslant T \leqslant 300\,\text{K}$. In addition, field sweeps between +40 kG and −40 kG were measured at various temperatures. The samples were contained in gelatin capsules fixed to the inside of a plastic straw for immersion into the SQUID. No diamagnetic corrections were made for the sample container because its signal was insignificant relative to that of the sample.

Table 3
Selected interatomic distances (Å) for $Ca_3Co_{1.34}Rh_{0.66}O_6$ and Ca_3FeRhO_6

	$Ca_3Co_{1.34}Rh_{0.66}O_6$	Ca_3FeRhO_6
M–O (×6)	2.111(1)	2.097(1)
Rh–O (×6)	1.968(1)	2.019(1)
Ca–O (×2)	2.335(1)	2.322(1)
Ca–O (×2)	2.495(1)	2.534(1)
Ca–O (×2)	2.503(1)	2.574(1)
Ca–O (×2)	2.592(2)	2.578(1)

Table 4
Selected interatomic distances (Å) for Ca_3CuRhO_6

Ca1–O1 (×2)	2.349(9)	Ca2–O2	2.355(9)
Ca1–O1 (×2)	2.459(12)	Ca2–O2	2.361(8)
Ca1–O2 (×2)	2.648(8)	Ca2–O1	2.368(8)
Ca1–O3 (×2)	2.660(8)	Ca2–O2	2.449(9)
		Ca2–O3	2.523(8)
Rh–O1 (×2)	1.960(9)	Ca2–O1	2.570(12)
Rh–O3 (×2)	2.001(7)	Ca2–O2	2.649(9)
Rh–O2 (×2)	2.001(9)	Ca2–O3	2.653(8)
Cu–O2 (×2)	1.996(9)		
Cu–O3 (×2)	1.998(8)		

2.4. *Scanning electron microscopy*

Scanning electron micrographs of several single crystal samples were obtained using a Philips XL 30 ESEM instrument utilized in environmental mode. Representative images of Ca_3CuRhO_6 emphasizing crystal morphology are shown in Fig. 3. The ESEM verified the presence of Ca, Cu, Co, Fe, and Rh and also, within the detection limits of the instrument, confirmed the absence of extraneous elements such as aluminum.

3. Results and discussion

3.1. *Crystal structure*

Black crystals of Ca_3CuRhO_6, $Ca_3Co_{1.34}Rh_{0.66}O_6$, and Ca_3FeRhO_6 were readily grown out of high temperature solutions of K_2CO_3. SEM micrographs showing representative crystal size and morphology are shown in Fig. 2. $Ca_3Co_{1.34}Rh_{0.66}O_6$ and Ca_3FeRhO_6 crystallize in the space group $R\bar{3}c$ with lattice parameters of $a = 9.161(1)$ Å, $c = 10.601(2)$ Å and $a = 9.1884(3)$ Å, $c = 10.7750(4)$ Å, respectively. Both are isostructural with the rhombohedral $m = 0$, $n = 1$ member of the $A_{3n+3m}A'_nB_{3m+n}O_{9m+6n}$ family, whose structure consists of infinite chains of alternating face-shared $[CoO_6]$ or $[FeO_6]$ trigonal prisms and $[RhO_6]$ octahedra separated by chains of calcium atoms, as shown in Fig. 1. The polyhedral chains run along [001] and are separated from each other by six chains of distorted $[CaO_8]$ square antiprisms. In the case of $Ca_3Co_{1.34}Rh_{0.66}O_6$, there is a 34% mixing of cobalt on the octahedral site while the trigonal prismatic site is occupied solely by cobalt. This composition, intermediate between that of Ca_3CoRhO_6 and $Ca_3Co_2O_6$, suggests that an entire solid solution can most likely be prepared. The lattice parameters of

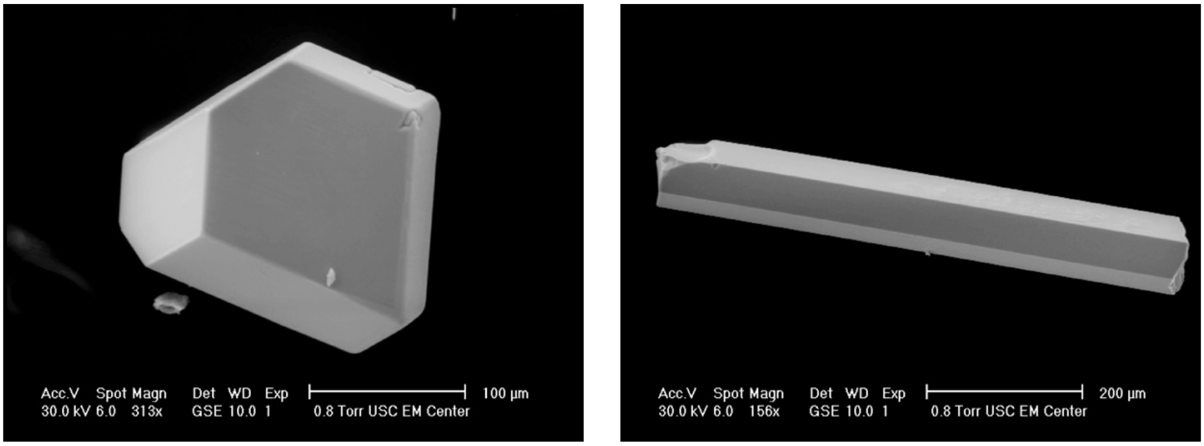

Fig. 2. SEM micrographs of Ca_3CuRhO_6.

Ca_3FeRhO_6 are within experimental error to those of the previously synthesized polycrystalline sample [39].

The incorporation of copper into the A' site results in ($A'O_4$) square planes rather than ($A'O_6$) trigonal prisms as in the previously mentioned structure. This is accomplished by the displacement of the copper atoms towards the faces of the trigonal prism, an effect previously observed in analogous copper containing compounds [5–16]. As a result of this displacement, the symmetry of Ca_3CuRhO_6 is lowered from rhombohedral to monoclinic, and consequently Ca_3CuRhO_6 crystallizes in the space group $C2/c$ with lattice parameters of $a = 9.004(2)\,\text{Å}$, $b = 9.218(2)\,\text{Å}$, $c = 6.453(1)\,\text{Å}$, $\beta = 91.672(5)$. Detailed crystallographic information for all compounds can be found in Tables 1–4.

3.2. Magnetic properties

The magnetic properties of this family of compounds have been investigated extensively and are interesting as well as complex, including random spin chain paramagnetism [9], antiferromagnetism [23,42–44], large magnetic anisotropies [36,45], and magnetic frustration [15,37]. In general, two groups of magnetic compounds exist in this family, those having unpaired electrons on both the trigonal prismatic and octahedral sites and those having unpaired electrons on only one of those sites. The materials discussed in this paper have metals with unpaired electrons occupying both the octahedral and trigonal prismatic (or square planar) sites, leading to significant magnetic interactions.

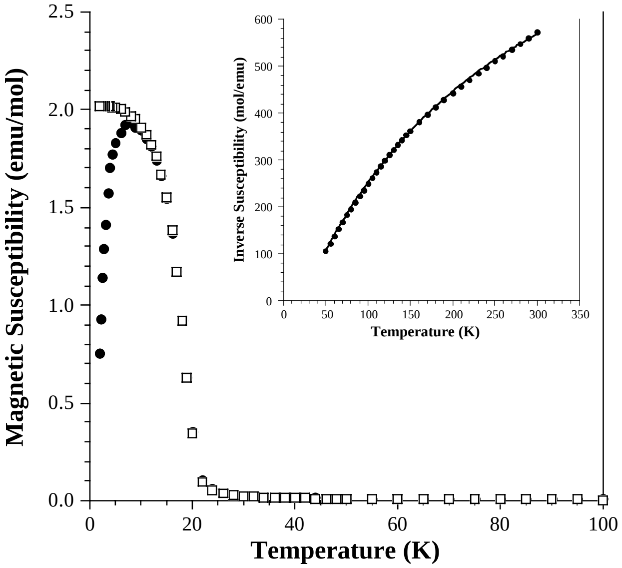

Fig. 3. Temperature dependence of the ZFC (●) and FC (□) magnetic susceptibility measured at an applied field of 500 G for Ca_3CuRhO_6. Inset: The inverse susceptibility as a function of temperature fit to the Curie–Weiss Law plus a TIP contribution is shown.

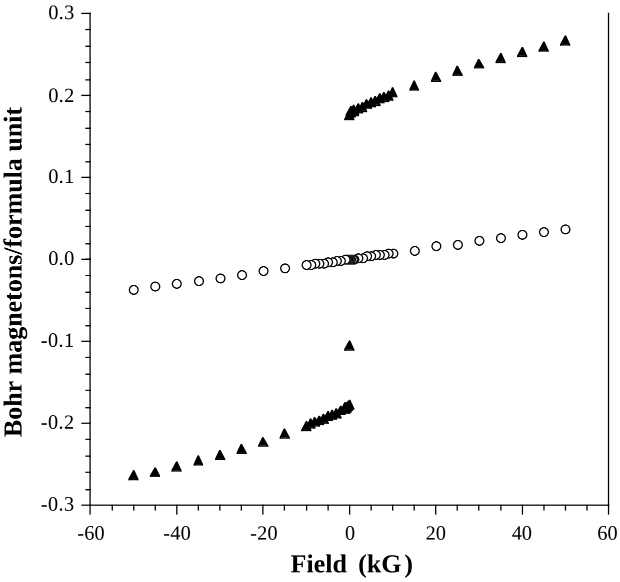

Fig. 4. Field dependence of the magnetization of Ca_3CuRhO_6 measured at 2 K (▲) and 100 K (○).

The magnetic susceptibility of Ca_3CuRhO_6 was measured in applied fields of 0.5, 5 and 40 kG. The 500 G measurement is shown in Fig. 3. The data follow Curie–Weiss type behavior at temperatures above 50 K. Fitting the high temperature data to the Curie–Weiss Law plus a TIP contribution, according to the equation $\chi = [C/(T-\theta)] + \text{TIP}$, yields a calculated effective moment of $1.42\,\mu_B$ ($\theta = 21\,\text{K}$; $\text{TIP} = 8.38 \times 10^4\,\text{emu mol}^{-1}$), which is lower than the theoretical spin-only moment for Rh^{4+} in an octahedral coordination and Cu^{2+} in a square planar coordination of $2.45\,\mu_B$. At high fields, both ZFC and FC data overlay down to the lowest temperature measured, 2 K. Only at very low applied fields (500 G or less), as shown, there is a clear separation between the ZFC and FC data collected. Whereas the FC data appear to be ordering ferromagnetically, the ZFC data undergo a second transition and below 5 K tend towards zero. Such deviations between the ZFC and the FC data are often indicative of geometric frustration or a spin glass state, which is possible in these materials due to their quasi-triangular structure.

The field dependence of the magnetization, shown in Fig. 4, indicates that at 2 K, Ca_3CuRhO_6 looks like a very soft ferromagnet. In fact, there is virtually no hysteresis observable. A careful analysis of the data, however, reveals that below about 500 G, there is a small hysteretic loop. Based on the data shown in Fig. 4, it is unlikely, however, that this represents the type of hysteresis observed for normal ferromagnetic materials. The M vs. H curve measured at 100 K, above the transition, shows no field dependence, as expected.

Very similar magnetic behavior has been observed for the closely related Sr_3CuRhO_6 [15] as well as for

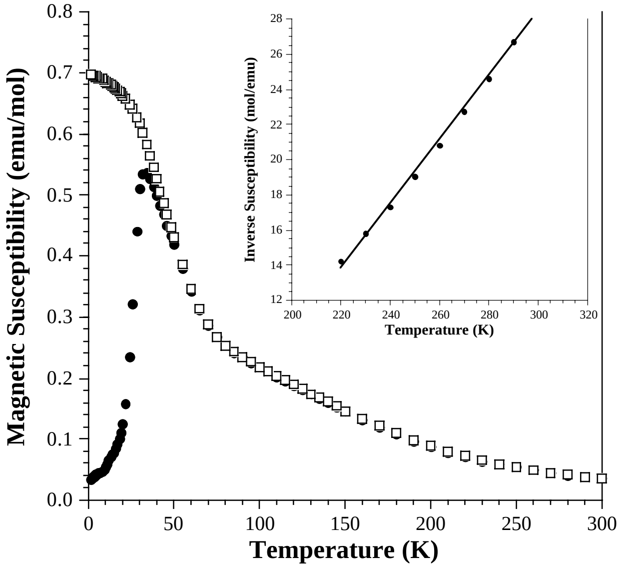

Fig. 5. Temperature dependence of the ZFC (●) and FC (☐) magnetic susceptibility measured at an applied field of 5 kG for $Ca_3Co_{1.34}Rh_{0.66}O_6$. Inset: The inverse susceptibility fit to the Curie–Weiss Law is shown.

Sr_3CuIrO_6 [10,46], which also has one unpaired electron for each of the octahedral and trigonal prismatic sites. Beauchamp and co-workers [46] recently carried out an investigation on the magnetic properties of Sr_3CuIrO_6, and found evidence for a 2-D ferromagnetic xy interaction in this material. This magnetic order is consistent with the temperature dependence of the susceptibility at low temperatures, and is followed by a 3-D magnetic transition below about 20 K. In addition, Sampathkumaran et al. recently investigated the $Sr_3Cu_{1-x}Zn_xIrO_6$ system and, based on AC susceptibility measurements, concluded that Sr_3CuIrO_6 exhibits spin glass behavior in zero field, but is driven toward a ferromagnetic state with reduced moment by the application of an applied field [11,47]. Given the almost identical field and temperature dependencies of these three materials, Ca_3CuRhO_6, Sr_3CuRhO_6, and Sr_3CuIrO_6, it is likely that the magnetic interactions are very similar in these compounds.

The magnetic susceptibility of $Ca_3Co_{1.34}Rh_{0.66}O_6$ (Fig. 5) is quite different, as far as the temperature dependence of the susceptibility is concerned. The magnetic susceptibility follows Curie–Weiss behavior at high temperatures, however below 200 K, there is a positive deviation from Curie–Weiss like behavior until 50 K, when the ZFC and FC data begin to diverge. The ZFC data exhibits a sharp drop around 32 K, while the FC data continue to increase and level off at approximately 25 K, very similar to what is observed for Ca_3CoRhO_6 and $Ca_3Co_2O_6$. The best fit of the high temperature (220–300°C) data to the Curie–Weiss law yields a Curie constant of 5.75 emu mol^{-1} K^{-1}, an effective moment of 6.76 μ_B and $\theta = 139$ K. However, it is important to point out that the values extracted from the magnetic data are dependent upon the chosen temperature range. The calculated Curie constant decreases to 4.78 emu mol^{-1} K^{-1} when the chosen temperature range is changed to 280–300°C, making it difficult to calculate a definitive moment. The positive Weiss constant, essentially invariant with the chosen temperature range, is consistent with the positive deviation from the Curie–Weiss law of the magnetic susceptibility data.

It is interesting to note that the measured magnetic moment for $Ca_3Co_{1.34}Rh_{0.66}O_6$ is unexpectedly high when compared to magnetic moments of 4.43 and 3.8 μ_B for Ca_3CoRhO_6 and $Ca_3Co_2O_6$, respectively, the two end-members of the $Ca_3Co_{1+x}Rh_{1-x}O_6$ series. Such a high magnetic moment is not unprecedented, as analogous compounds of this family that contain cobalt in the trigonal prismatic site have also yielded high magnetic moments [48]. Nonetheless, while it is quite likely that this high moment is due to spin orbit coupling of the cobalt on the trigonal prismatic sites, the uncertainty over the values of the oxidation states for cobalt and rhodium and their distribution over the two sites precludes a detailed analysis at this time.

The general shape of the magnetic susceptibility curve of $Ca_3Co_{1.34}Rh_{0.66}O_6$ is very similar to those reported for Ca_3CoRhO_6 and $Ca_3Co_2O_6$. This is not really unexpected as compositionally $Ca_3Co_{1.34}Rh_{0.66}O_6$ is an intermediate between the two. Both Ca_3CoRhO_6 and $Ca_3Co_2O_6$ consist of triangular lattices of ferromagnetic chains that couple antiferromagnetically, possibly causing magnetic frustration [18,49,50]. Recent work by Niitaka et al. further examined the complex magnetic behavior of Ca_3CoRhO_6 and showed by high-field magnetization experiments and neutron diffraction studies that Ca_3CoRhO_6 realizes a partially disordered antiferromagnetic (PDA) state [49,50]. Between 30 and 90 K, $\frac{2}{3}$ of the ferromagnetic chains order antiferromagnetically with each other, while the remaining $\frac{1}{3}$ are proposed to be left incoherent with the other chains. Interestingly, $Ca_3Co_2O_6$ does not exhibit a PDA state. Further studies on $Ca_3Co_{1.34}Rh_{0.66}O_6$ are required to reveal the exact nature of the magnetic behavior of this intermediate in the $Ca_3Co_{1+x}Rh_{1-x}O_6$ series.

The magnetic susceptibility of Ca_3FeRhO_6 was measured and shows Curie–Weiss behavior above 50 K. The susceptibility reaches a maximum at 13 K, followed by a downturn, indicative of an antiferromagnetic transition, which is in agreement with the negative Weiss temperature of –30 K. This transition is followed by an increase in susceptibility at 11 K and continues to the lowest measured temperature of 2 K. The ZFC and FC data overlay in the entire temperature range and are identical to the previously reported polycrystalline samples [39].

4. Conclusion

In summary, the molten flux approach continues to be an extremely effective method for growing single crystals of this oxide family, where it has been demonstrated that both single crystals of the $A_3A'BO_6$ structure-type, and more complex structural modifications [1] can be obtained. Single crystals of Ca_3CuRhO_6, $Ca_3Co_{1.34}Rh_{0.66}O_6$ and Ca_3FeRhO_6 were grown from high temperature solutions of K_2CO_3. While $Ca_3Co_{1.34}Rh_{0.66}O_6$ and Ca_3FeRhO_6 crystallize in the rhombohedral K_4CdCl_6 structure type, Ca_3CuRhO_6 adopts the monoclinic distortion of that structure type. The magnetic properties of Ca_3CuRhO_6 were examined and found to be consistent with that of a soft ferromagnet with a lower than expected effective magnetic moment. $Ca_3Co_{1.34}Rh_{0.66}O_6$ exhibits magnetic data consistent with the presence of ferromagnetic correlations within the chains. Ca_3FeRhO_6 exhibits simple antiferromagnetic type behavior. Work is continuing on the growth of crystals with novel compositions related to the 2H-perovskite family of oxides.

Acknowledgment

Financial support for this research was provided by the National Science Foundation through Grant DMR:0134156.

Supplemental Data

Further details of the crystal structure investigations can be obtained from the Fachinformationszentrum Karlsruhe, 76344 Eggenstein-Leopoldshafen, Germany, (fax: (49) 7247-808-666; e-mail: mailto:crysdata@fiz-karlsruhe.de) on quoting the depository numbers CSD-412848-412850.

References

[1] K.E. Stitzer, J. Darriet, H.-C. zur Loye, Curr. Opin. Solid State Mater. Sci. 5 (2001) 535.
[2] J. Darriet, M.A. Subramanian, J. Mater. Chem. 5 (1995) 543.
[3] J.M. Perez-Mato, M. Zakhour-Nakhl, F. Weill, J. Darriet, J. Mater. Chem. 9 (1999) 2795.
[4] J.J. Randall, L. Katz, Acta Crystallogr. 12 (1959) 519.
[5] J.B. Claridge, R.C. Layland, W.H. Henley, H.-C. zur Loye, Chem. Mater. 11 (1999) 1376.
[6] W.H. Henley, J.B. Claridge, P.L. Smallwood, H.-C. zur Loye, J. Cryst. Growth 204 (1999) 122.
[7] C.A. Moore, E.J. Cussen, P.D. Battle, J. Solid State Chem. 153 (2000) 254.
[8] M. Neubacher, Hk. Müller-Buschbaum, Z. Anorg. Allg. Chem. 607 (1992) 124.
[9] T.N. Nguyen, P.A. Lee, H.-C. zur Loye, Science 271 (1996) 489.
[10] T.N. Nguyen, H.-C. zur Loye, J. Solid State Chem. 117 (1995) 300.
[11] A. Niazi, E.V. Sampathkumaran, P.L. Paulose, D. Eckert, A. Handstein, K.-H. Müller, Solid State Commun. 120 (2001) 11.
[12] A. Tomaszewska, Hk. Müller-Buschbaum, Z. Anorg. Allg. Chem. 619 (1993) 534.
[13] A. Tomaszewska, Hk. Müller-Buschbaum, Z. Anorg. Allg. Chem. 617 (1992) 23.
[14] A.P. Wilkinson, A.K. Cheetham, W. Kunnman, Å. Kvick, Eur. J. Solid State Inorg. Chem. 28 (1991) 453.
[15] K.E. Stitzer, W.H. Henley, J.B. Claridge, H.-C. zur Loye, R.C. Layland, J. Solid State Chem. 164 (2002) 220.
[16] J.L. Hodeau, H.Y. Tu, P. Bordet, T. Fournier, P. Strobel, M. Marezio, G.V. Chandrashekhar, Acta Crystallogr. B 48 (1992) 1.
[17] D. Elwell, H.J. Scheel, Crystal Growth from High-Temperature Solutions, Academic Press, New York, 1975.
[18] A. Maignan, C. Michel, A.C. Masset, C. Martin, B. Raveau, Eur. Phys. J. B 15 (2000) 657.
[19] A. El Abed, E. Gaudin, S. Lemaux, J. Darriet, Solid State Sci. 3 (2001) 887.
[20] J.A. Campá, E. Gutiérrez-Puebla, M.A. Monge, I. Rasines, C. Ruíz-Valero, J. Solid State Chem. 108 (1994) 230.
[21] M. Evain, F. Boucher, O. Gourdon, V. Petricek, M. Dusek, P. Bezdicka, Chem. Mater. 10 (1998) 3068.
[22] B.A. Reisner, A.M. Stacy, J. Am. Chem. Soc. 120 (1998) 9682.
[23] T.N. Nguyen, D.M. Giaquinta, H.-C. zur Loye, Chem. Mater. 6 (1994) 1642.
[24] J.B. Claridge, R.C. Layland, W.H. Henley, H.-C. zur Loye, Z. Anorg. Allg. Chem. 624 (1998) 1951.
[25] M.D. Smith, J.K. Stalick, H.-C. zur Loye, Chem. Mater. 11 (1999) 2984.
[26] M.J. Davis, M.D. Smith, H.-C. zur Loye, Acta Crystallogr. C 57 (2001) 1234.
[27] H.-C. zur Loye, R.C. Layland, M.D. Smith, J.B. Claridge, J. Cryst. Growth 211 (2000) 452.
[28] J.B. Claridge, R.C. Layland, H.-C. zur Loye, Acta Crystallogr. C 53 (1997) 1740.
[29] M.J. Davis, M.D. Smith, K.E. Stitzer, H.C. zur Loye, J. Alloys Compd. 351 (2003) 95.
[30] J.B. Claridge, R.C. Layland, R.D. Adams, H.-C. zur Loye, Z. Anorg. Allg. Chem. 623 (1997) 1131.
[31] M.D. Smith, H.-C. zur Loye, Acta Crystallogr. C 57 (2001) 337.
[32] K.E. Stitzer, M.D. Smith, J. Darriet, H.-C. zur Loye, Chem. Commun. 1680 (2001).
[33] S. Aasland, H. Fjellvåg, B. Hauback, Solid State Commun. 101 (1997) 187.
[34] H. Fjellvåg, E. Gulbrandsen, S. Aasland, A. Olsen, B.C. Hauback, J. Solid State Chem. 124 (1996) 190.
[35] H. Kageyama, K. Yoshimura, K. Kosuge, J. Solid State Chem. 140 (1998) 14.
[36] H. Kageyama, K. Yoshimura, K. Kosuge, M. Azuma, M. Takano, H. Mitamura, T. Goto, J. Phys. Soc. Japan 66 (1997) 3996.
[37] H. Kageyama, K. Yoshimura, K. Kosuge, H. Mitamura, T. Goto, J. Phys. Soc. Japan 66 (1997) 1607.
[38] H. Kageyama, K. Yoshimura, K. Kosuge, X. Xu, S. Kawano, J. Phys. Soc. Japan 67 (1998) 357.
[39] S. Niitaka, H. Kageyama, M. Kato, K. Yoshimura, K. Kosuge, J. Solid State Chem. 146 (1999) 137.
[40] SMART Version 5.624, SAINT+ Version 6.02a and SADABS; Bruker Analytical X-ray Systems, Inc.: Madison, Wisconsin, USA, 1998.
[41] G.M. Sheldrick, SHELXTL Version 5.1; Bruker Analytical X-ray Systems, Inc.: Madison, Wisconsin, USA, 1997.

[42] N. Segal, J.F. Vente, T.S. Bush, P.D. Battle, J. Mater. Chem. 6 (1996) 395.

[43] R.C. Layland, H.C. zur Loye, Mat. Res. Bull. 36 (2001) 2701.

[44] S. Kawasaki, M. Takano, T. Inami, J. Solid State Chem. 145 (1999) 302.

[45] H.-C. zur Loye, K.E. Stitzer, M.D. Smith, A. El Abed, J. Darriet, Inorg. Chem. 40 (2001) 5152.

[46] S.H. Irons, T.D. Sangrey, K.M. Beauchamp, M.D. Smith, H.-C. zur Loye, Phys. Rev. B 61 (2000) 11594.

[47] A. Niazi, E.V. Sampathkumaran, P.L. Paulose, D. Eckert, A. Handstein, K.-H. Müller, Phys. Rev. B 65 (2001) 180401.

[48] T.N. Nguyen, H.-C. zur Loye, in: D.A.Neumann, T.P. Russel, B.J. Wuensch (Eds.), Neutron Scattering in Materials Science, Vol. 376, MRS Symposia Proceedings, 1995, p. 603.

[49] S. Niitaka, H. Kageyama, K. Yoshimura, K. Kosuge, S. Kawano, N. Aso, A. Mitsuda, H. Mitamura, T. Goto, J. Phys. Soc. Japan 70 (2001) 1222.

[50] S. Niitaka, K. Yoshimura, K. Kosuge, M. Nishi, K. Kakurai, Phys. Rev. Lett. 87 (2001) 177202.